Available online at www.sciencedirect.com
ScienceDirect
Journal of Catalysis 243 (2006) 158–164
JOURNAL OF CATALYSIS
www.elsevier.com/locate/jcat

CO desorption and oxidation on CeO_2-supported Rh: Evidence for two types of Rh sites

Jun Xu, David R. Mullins, S.H. Overbury *

Chemical Sciences Division, Oak Ridge National Laboratory, Oak Ridge, TN 37831-6201, USA

Received 14 March 2006; revised 31 May 2006; accepted 11 July 2006

Available online 24 August 2006

Abstract

Previous co-adsorption studies of CO and oxygen on Rh single-crystal surfaces have shown that formation of CO_2 is the dominant pathway during temperature-programmed desorption and that the reaction limits the competing pathway of CO and O_2 desorption. The present work finds that this selectivity is altered on CeO_2-supported Rh islands. In addition to facile CO oxidation, a new CO adsorption state is found that is associated with the Rh but is observed only in the presence of both the CeO_2 support and pre-adsorbed oxygen. This state is characterized by its low desorption temperature (140–250 K), well below the CO_2 formation temperatures of 290 K (β_2) and 360 K (β_1), and by its IRAS frequency of 2100 cm^{-1}, higher than observed for either CO adsorbed on the supported Rh islands (2057–2066 cm^{-1}) or CO co-adsorbed with O on Rh islands (2074 cm^{-1}). The data suggest that oxygen and subsequent CO exposure of CeO_2 supported Rh creates atomically dispersed *gem*-dicarbonyl, $Rh(CO)_2$, from the edge of Rh islands. As temperature increases, part of the dicarbonyl desorbs at low temperature, and the remainder is converted to CO_2. The low-temperature desorption pathway has a selectivity as high as 46%, with the remaining CO oxidized to CO_2.

Keywords: CO oxidation; Oxidation catalysis; Adsorption; RAIRS; IRAS; XPS; TPD; Ru; Rh; CeO_2; Cerium oxide

1. Introduction

CO oxidation on noble metals has been exhaustively studied on single-crystal metals, particularly Rh [1–5]. Practical interest in this reaction relates to automotive exhaust catalysis and the efficient conversion of exhaust CO and NO. At low coverage, the Langmuir–Hinshelwood mechanism seems appropriate to explain CO oxidation; consequently, many studies have examined the co-adsorption of CO and oxygen [6]. In temperature-programmed desorption (TPD), two CO_2 TPD peaks, denoted by β_1 (460 K) and β_2 (390 K), were observed for CO oxidation on an oxygen pre-exposed Rh(111) surface [2]. Similar features were observed for CO on O pre-exposed Rh(100) [7] and Pt(111) [4]. Yoshinobu et al. [4] demonstrated a link between β_1 and β_2 and various oxygen structures on the surface. β_1-CO_2 formation occurs for both disordered and (2×2) ordered oxygen sites. At a low CO coverage, β_1 oxidation dominates. At higher CO coverage, β_2-CO_2 formation occurs. β_2 can be indicative of a repulsive interaction in the adsorbed CO layer. Differences are observed in the behavior of co-adsorbed CO and oxygen that depend on the structure or orientation of the crystal faces. Hopstaken and Niemantsverdriet demonstrated that the CO oxidation rate on Rh(100) is 10 times higher than that for Rh(111) [8] under TPD conditions. In higher pressure reactor-based measurements, CO oxidation reaction rates are also sensitive to surface structure [9] under oxygen-rich conditions, but under conditions where the surface is largely covered by CO, the reaction rates are insensitive to structure [3,8].

Additional information about the adsorption and oxidation of CO can be obtained by soft X-ray photoemission [10–12] or by probing the stretching frequency of the CO by infrared absorption spectroscopy (IRAS) [13–15] or by high-resolution electron energy loss spectroscopy (HREELS) [7,16–18]. The stretching frequency of the CO may be affected by the structure of the CO bonding site, by dipole interactions between neighboring CO molecules, or by chemical interactions with atoms on neighboring sites that may alter the strength of the

* Corresponding author.
E-mail address: overburysh@ornl.gov (S.H. Overbury).

0021-9517/$ – see front matter
doi:10.1016/j.jcat.2006.07.008

CO bond. The nature of CO adsorption sites or the effect of neighboring oxygen on the CO thus may be probed by IRAS. For a clean Rh(111) surface and CO saturation coverage, the CO stretching frequency observed by IRAS is 2067 cm^{-1} for the on-top site and 1860 cm^{-1} the three-fold hollow sites [19], whereas for a Rh(100) surface, the CO stretching frequencies are observed at 2062 and 1942 cm^{-1} for on-top and bridge-bonded sites, respectively [14]. Although interactions between CO and oxygen on single-crystal Rh surfaces have been studied by HREELS [7], we could not find literature regarding the use of IRAS experiments to probe this interaction.

Compared with single-crystal Rh surfaces, less work has been done on CO adsorption and oxidation by Rh particles supported on single-crystal oxides. Oxide-supported metal particles may behave differently that unsupported metal surfaces because supports bring additional types of interactions that affect reaction selectivity of catalysts. These extra interactions may bring about changes in physical, structural, and electronic properties of both the oxide support and the metal particle [20]. Such effects are well known on CeO_2 surfaces [21]. On CeO_2-supported metal particles, the dissociation probability of CO [22–25] or NO [26] depends on the extent of reduction of the CeO_2 or on the nature of underlying films. CO_2 formation over metal particles depends on the structure of the CeO_2 support [23]. Presence of a ceria support promotes the CO methanation reaction on Rh particles [27]. Various mechanisms by which the support may affect oxidation reactions have been proposed. The support may affect the structure of the supported metals and thus alter the bonding energetics. It may also provide a source of active oxygen that can contribute to the oxidation of CO, augmenting O adsorbed on the metal [23]. Another mechanism is electron transfer from defects, as occurs for Au particles adsorbed on MgO that contain adsorbed CO and O_2. In this case the electrons supplied by the F centers of the oxide support strengthens the bond between CO and the metal particles [28].

To investigate further support effects in oxidation reactions occurring on metal particles, as related to reactivity and selectivity of catalysts, we studied co-adsorption and reaction of CO and oxygen on CeO_2-supported Rh particles. We present evidence for a CO adsorption state induced by oxygen pre-exposure on Rh/CeO_2. CO in this state preferentially desorbs, rather than react with co-adsorbed O ad-atoms, thereby altering the reaction selectivity. This CO state is proposed to be *gem*-dicarbonyl on isolated Rh sites, dispersed by oxygen exposure at the edges of Rh islands.

2. Experimental

Experiments were performed in two UHV systems. One system was equipped for XPS, TPD, and reflection mode IRAS in a side chamber. A second system (the TPD system), with essentially identical sample preparation capabilities, was used for auxiliary TPD experiments, because it exhibited lower background pressure during TPD experiments. A Ru(0001) surface was used as a substrate for growth of CeO_2 films [22]; it was cleaned by sputtering followed by annealing at 900 K. The CeO_2 surface was synthesized by Ce vapor deposition in an oxygen environment on the Ru (0001) surface that was maintained at 700 K. Ce was vaporized by passing current through a pair of W wires supporting a Ta envelope, which contained Ce metal and had an aperture directed at the Ru substrate. Ce deposition was performed in O_2 pressure typically ranging from 5×10^{-9} to 5×10^{-7} Torr. The deposited film was annealed in O_2 up to 900 K and then cooled to 500 K in O_2 before stopping the O_2 flow and cooling to room temperature. The oxidation state of the ceria film (i.e., the ratio of Ce^{3+} to Ce^{4+}) was measured by curve fitting the XPS of the Ce 3d states [29]. By controlling the oxygen pressure, the oxidation state was varied from about 98% Ce^{4+} to about 33% Ce^{4+}, denoted as $CeO_{1.99}$ to $CeO_{1.67}$. Film thickness was typically in a range of few nanometers.

Rh was deposited on the CeO_2 surface at 300 K as described previously [30]. After deposition, the surface was annealed at 800–900 K for 30 s. Rh deposition on the CeO_2 surface consistently caused a slight (<5%) measured reduction of the cerium oxide. From comparison of the Rh XPS intensity with the intensity obtained from clean Ru(0001), the rate of deposition in the IRAS system was estimated to be about 1.3 Rh/(nm^2 min), or about 0.08 ML/min defined in terms of a Rh(111) monolayer [30]. The Rh deposition rate in the TPD system should be comparable to that in the IRAS chamber. In this system, Rh coverage was estimated from comparing the Rh/Ce Auger ratio and the deposition time. Although the total amount of Rh deposited was not well calibrated, the amount of surface Rh was assessed by CO adsorption as follows. After each Rh deposition, CO was adsorbed to saturation at room temperature, and TPD was performed to determine the amount of CO adsorbed. CO TPD spectra from the CeO_2 before Rh deposition were measured and subtracted as a background from the spectra obtained when Rh was present. No CO_2 desorption was observed from the Rh-free CeO_2 surface. Integrated CO desorption intensity was calibrated separately by measuring the desorption yield from CO-saturated Ru(0001), assumed to correspond to 9.2 CO/nm^2 [31]. CO saturation on the Rh particles was assumed to be 12 CO/nm^2, based on the saturation density on Rh(111) [32]. Integrated CO intensity from the Rh islands was then related to the fraction of the CeO_2 covered by the Rh particles. Fractional coverages for typical Rh depositions following four different dosing times are shown in Table 1.

For chemisorption experiments, the Rh/CeO_2 surface was typically cooled to 100 K, and then the surface was exposed to O_2 by backfilling the UHV chamber. The oxygen exposure

Table 1
TPD yield of the low temperature CO and CO_2 as a function of Rh deposition

Rh deposition time (min)	15	12	10	7
Auger ratio, Rh/Ce	0.23	0.18	0.17	0.14
Rh fractional coverage[a]	0.53	0.42	0.37	0.24
$^{13}C^{16}O$ areal density on Rh (molecules/nm^2)[b]	1.09	0.95	0.97	0.79
CO_2 areal density on Rh (molecules/nm^2)[b]	1.30	1.17	1.22	1.29
CO/CO_2	0.85	0.80	0.78	0.61

[a] Estimated from CO desorption from O-free Rh particles.
[b] From TPD, normalized to Rh fractional coverage; (density of CO or CO_2 on Rh particles).

also oxidized the outermost layer of the ceria film, which was reduced slightly during Rh deposition. Previous XPS results indicate that although the Rh 3d peak was shifted 0.3 eV to higher binding energy by oxygen exposure, the Rh was not oxidized under these conditions [30]. To distinguish bulk oxygen from dosed oxygen, $^{18}O_2$ was used for oxygen pre-exposure and $^{16}O_2$ was used for generating CeO_2 films. CO dosing was conducted with two methods: direct dose and backfill. Direct CO dosing was done by facing the surface to one end of a 12-mm-i.d. tube connected through a pinhole to a ballast volume of CO. The CO backing pressure on the source side of the pinhole was typically about 0.4 Torr, resulting in a pressure of 7×10^{-8} Torr in the dosing tube, if the end of the tube is blocked by the sample. Dosing by backfilling was conducted simply by leaking CO into the UHV. After dosing and before TPD, filament wires were flash-heated without significantly heating the sample, to reduce the interference of desorption from the heating wires. The chamber pressure was then allowed to drop again before TPD was initiated.

A Mattson IR spectrometer was used for the reflection absorption infrared spectroscopy. A wedge shaped sample holder was used to reduce light reflected from it. IRAS spectra were measured with 4 cm^{-1} resolution and averaged over 500 scans at an incident angle is about 6°. The XPS experiments were described previously [30]. The X-ray incidence and electron detection angles were 45° from the sample surface.

3. Results

Fig. 1 shows IRAS spectra of CO on Rh islands supported on a reduced cerium oxide for various CO exposures without oxygen pre-exposure. The starting ceria support was reduced ($CeO_{1.83}$) and the total amount of Rh was 18 nm^{-2}. Both CO exposure and IRAS measurements were conducted at room temperature. Similar to single-crystal surface Rh(111), the CO atop stretching frequency increased with increasing CO coverage and saturated at 2067 cm^{-1}, the same frequency as for the Rh(111) crystal surface [19]. This correspondence suggests that much of the Rh particle behaved like a Rh(111) facet. No linearly bonded CO was seen when CO was exposed to the fully oxidized CeO_2 before Rh deposition, although carbonates or carboxylates may have been present, as demonstrated previously by SXPS [22].

The saturation frequency for supported Rh was found to depend on the oxidation state of the ceria support and the amount of Rh deposition. When Rh coverage was fixed near 10 nm^{-2}, the saturation frequency decreased with decreasing oxidation state, observed at 2063, 2050, and 2042 cm^{-1} for mean oxidation states of $CeO_{1.95}$, $CeO_{1.83}$, and $CeO_{1.67}$, respectively. This change in the stretching frequency reflects the effect of the support on defining the properties of the Rh particle. Previous reports have indicated that reduction of ceria leads to increased dissociation of CO on supported Rh particles above room temperature [22]. This effect, which led to enhanced CO dissociation, whether electronic or structural, evidently also led to weakening of the CO stretching frequency in the undissociated, adsorbed CO. For a fixed oxidation state, the saturation frequency was also found to decrease with Rh coverage, from 2067 to 2042 cm^{-1}, as the Rh coverage dropped from about 32 to 8 nm^{-2} for a surface with mean oxidation state equivalent to $CeO_{1.67}$. With decreasing Rh coverage, the particles deviated further from the behavior of a Rh(111) surface, suggesting changes in the size of the Rh particles.

Fig. 2 shows IRAS spectra for CO adsorbed on a 1.2 L O_2 pre-exposed Rh/CeO_2 surface. Before the oxygen pre-exposure, the ceria support was mostly oxidized with >95% Ce^{4+} ($CeO_{1.975}$). The Rh/CeO_2 surface was then exposed to O_2 at 100 K, followed by CO saturation exposure at 100 K. Finally, the surface was annealed sequentially to the listed temperatures

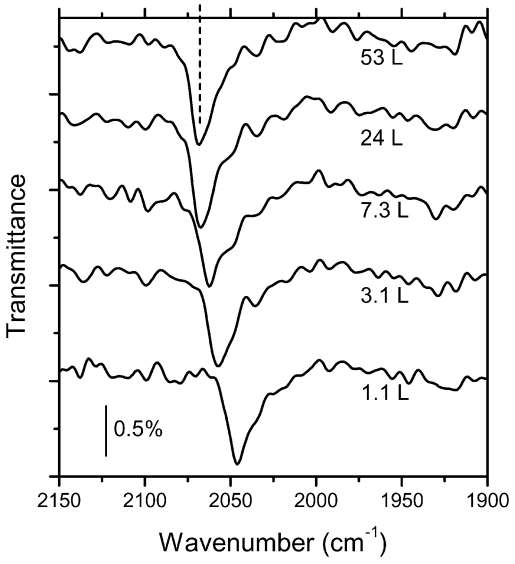

Fig. 1. IRAS spectra for various CO exposures on a Rh/CeO_x surface. Dosing and IR experiments were done at room temperature. Dashed line at 2067 cm^{-1} indicates frequency of the peak at saturation.

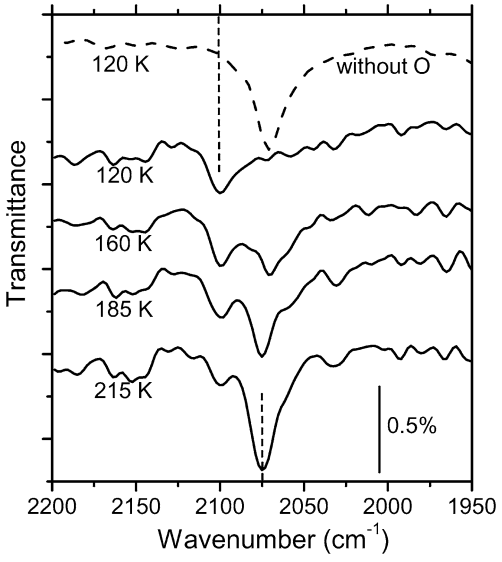

Fig. 2. IRAS spectra as a function of annealing temperature for CO on clean (top curve only) and oxygen pre-exposed Rh particles supported on CeO_2. Oxygen pre-exposure was 1.2 L. All the spectra were measured at 120 K after annealing at the indicated temperature for 30 s.

for 30 s. All IRAS measurements were performed after cooling to 120 K. As shown in the spectra, two CO IRAS peaks are indicated by dashed lines: one peak at 2100 cm^{-1} observed only in a low-temperature range of 120 to about 215 K and a second peak at 2070–2075 cm^{-1} for a temperature in the range 160–400 K. The top curve in Fig. 2 (dashed curve) shows a CO saturated surface that was prepared similarly, except not pre-exposed with O_2.

The high-frequency peak near 2100 cm^{-1} was observed only in the low-temperature range. Its intensity decreased with increasing annealing temperature, but the frequency did not vary. This state cannot be associated with multicoordinating sites (bridged site and hollow site) of Rh, because these frequencies are always observed at much lower frequencies, around 1860–1940 cm^{-1} [14]. The new frequency here was higher (by >30 cm^{-1}) than even the linear bonded frequency observed on Rh(111). It was absent when O_2 was not dosed before CO exposure, as illustrated by the topmost curve in Fig. 2. In this spectrum, there is no evidence for the high-frequency CO peak. In the reverse circumstances when CO was dosed first, or when both O_2 and CO were co-dosed at the same time, the 2100 cm^{-1} peak was not clearly seen. We also found evidence that this new peak must be associated with the presence of the CeO_2 layer because it was not observed for adsorption of CO on O pre-exposed Rh islands supported by the Ru(0001) substrate. This frequency was close to the 2107 cm^{-1} observed for *gem*-dicarbonyl adsorbed on Rh atomically dispersed on SiO_2 or Al_2O_3 [33]. Frank et al. [34] also reported *gem*-dicarbonyl at 2120 cm^{-1} obtained when small Rh particles (containing 9–30 atoms) are present on flat, low-surface area Al_2O_3 films. Based on these results, the 2100 cm^{-1} peak is assigned to dicarbonyl adsorbed on small Rh particles or on atomically dispersed Rh created by the oxygen exposure of Rh islands supported by CeO_2.

The low-frequency peak near 2072 cm^{-1} is attributed to the linearly bonded CO embedded into oxygen domains on the Rh islands. On Rh(111), the oxygen ad-atoms occupy hollow sites at about $\frac{1}{4}$ ML coverage, whereas CO occupies on-top sites within the oxygen domains [13,35]. Interestingly, the linearly adsorbed CO frequency was not clearly observed at 120 K, but appeared after annealing to 160 K. We attribute this appearance to conversion of the *gem*-carbonyl to a linear bonded state with a single CO bonded to Rh. Because the dicarbonyl is expected to be stable on isolated Rh up to 300 K or higher [33], the conversion may occur as a result of low-temperature removal of oxide defects that stabilize the isolated Rh *gem*-dicarbonyl [34]. This conversion explains both the loss of the high-frequency peaks and the simultaneous growth of the low-frequency peaks. At 160 and 215 K, the low-frequency CO peak was observed at about 2072 cm^{-1}, which was blue-shifted relative to CO on Rh islands or on Rh(111) without O adsorption. This blue shift is attributed to chemical interactions between co-adsorbed O and CO that weakens the Rh–CO bond and, by the Blyholder model [36], strengthens the RhC–O bond. A similar blue shift occurs when CO is co-adsorbed with O on Rh(100) [7] and on Pt(111) [4].

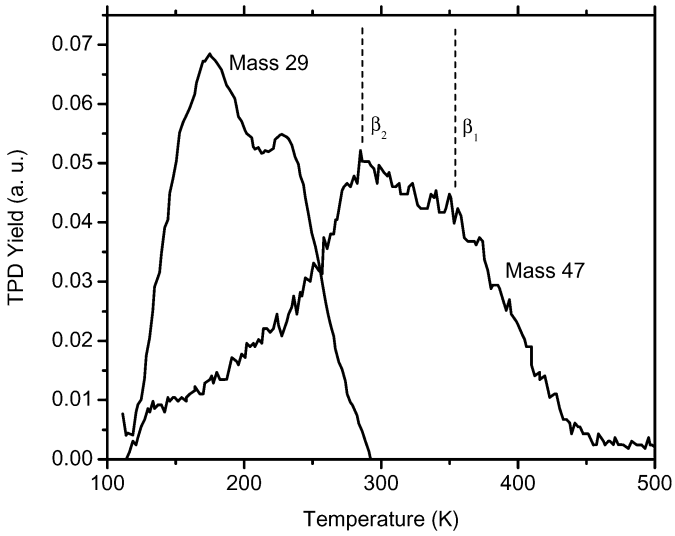

Fig. 3. TPD spectra of mass 29 and mass 47 for the Rh/CeO_2 surface. The surface was pre-exposed with $^{18}O_2$ and then exposed to $^{13}C^{16}O$. Rh deposition: 15 min (see Table 1), O_2: 1.5 L at 100 K, CO saturation coverage. Mass 29 desorption spectrum was corrected by subtraction of a background desorption spectrum obtained from CO exposed CeO_2.

Fig. 3 shows TPD spectra of CO_2 and CO from CO adsorbed on O pre-exposed Rh/CeO_2 surfaces. O_2 was pre-exposed at 100 K followed by heating at 200 K for 30 s before cooling to 100 K for CO adsorption. To minimize the background interference, $^{18}O_2$ and $^{13}C^{16}O$ were used for O_2 and CO exposures. Two desorption features are observed: CO desorption (mass 29) in a temperature range of 120–285 K and broad CO_2 (mass 47, $^{13}C^{16}O^{18}O$) formation at temperatures of 200–400 K. If the surface was not annealed to 200 K after the O_2 pre-exposure, then molecular O_2 was also observed to desorb below 200 K.

The CO desorption (mass 29) in a temperature range of 120–285 K observed for the supported Rh particles is not seen from single-crystal Rh surfaces [2]. For Rh single-crystal surfaces, CO desorption occurred near 400–500 K, but this CO desorption channel was supplanted by CO_2 desorption when co-adsorbed O was present. For the supported Rh particles, however, the yield of desorbed CO was comparable to the yield of desorbed CO_2. Desorption and oxidation of CO were competing pathways during the temperature increase. The ratio of the total amount of CO desorbed (140–250 K) to the CO oxidized in the temperature range of 200–450 K was measured as a function of Rh coverage (see Table 1). The amounts of CO and CO_2 desorbed were calibrated as described above and normalized to the Rh fractional coverage, thereby providing the density of CO on the Rh particles. It can be seen that roughly equal amounts of CO were oxidized and desorbed, with a small variation based on Rh coverage. The variation in this ratio was likely related to variation in the population of structurally different types of sites responsible for the two different pathways. For example, the ratio of island edge sites to island terrace sites might be expected to vary with Rh coverage, and these two sites could interact differently with CO.

The observed low-temperature desorption correlated with the temperature range in which the 2100 cm^{-1} IRAS peak

was observed, demonstrating that both this peak and the low-temperature CO desorption came from the same state of CO on the surface. Such a high IRAS frequency indicates a weak bond between the CO and the surface consistent with the low-temperature desorption. Further experiments demonstrated that the low-temperature desorption was not observed if CO was dosed before O_2 or if CO and O_2 were dosed at the same time, similar to the case with the 2100 cm^{-1} IRAS peak.

CO_2 desorption apparently had two components peaking near 290 and 360 K, designated as β_2 and β_1, respectively. For Rh(111), CO_2-β_1 formation resulted from interaction of CO and O on the perimeters of CO and O domains, whereas CO_2-β_2 formation was attributed to CO mixed into O domains [37]. Because oxygen exposure occurred before CO exposure, we would expect O to cover the surface, generating mixed domains, and thus expect β_2 formation to be the more intense peak. For similar heating rates, these desorption temperatures were about 100 K lower than the β_1 and β_2 CO_2 formation temperatures reported for CO adsorption on O_2 pre-exposed Rh(111), and more comparable with those on O_2 pre-exposed Rh(100) surfaces [8]. Matsushima et al. have shown that polycrystalline Rh yields CO_2 desorption peaks at lower temperatures than Rh(111) [2,37]. They suggested that the lower desorption temperature on the polycrystalline surfaces could be attributed to steps [2]. Because the Rh particles seem to behave like (111) facets before oxygen exposure, comparison of the desorption temperatures suggest that oxygen adsorption introduced roughening of the surfaces of the Rh islands.

As mentioned above, O_2 desorbs in the 100–200 K range. The question arises as to whether the high-frequency IRAS state (2100 cm^{-1} in Fig. 2) could be caused by the presence of adsorbed O_2. To check this, the experiments described in Fig. 2 were repeated, except that oxygen pre-exposure was performed at 300 K, where no nondissociative adsorption occurred. Fig. 4 shows the IRAS spectra following this procedure. Clearly, the high-frequency CO state was again present in the low-temperature range. Obviously, oxygen ad-molecules were not a factor for formation of the CO state at 2100 cm^{-1}. In fact, the intensity of the high-frequency CO generated following after the 300 K oxygen pre-exposure was higher than that for the 110 K O_2 pre-exposure, as shown in Fig. 5, which compares the intensity of the of the CO peak for oxygen pre-exposures at the two temperatures. In both cases, the low-frequency peak was not visible after CO exposure at 120 K but grew with increasing annealing temperature (compare Figs. 2 and 4). However, in the case of the high-temperature oxygen pre-exposure (Fig. 4), the low-frequency peak appeared as a shoulder, and the evolution of the spectrum with temperature was complex. This complexity suggests site inhomogeneity, possibly caused by disordering or restructuring during the high-temperature oxygen pre-exposure. CeO_2 has been found to be a factor in formation of the 2100 cm^{-1} CO adsorption state. This was tested by performing similar experiments on a surface with about 10 nm^{-2} Rh deposited directly onto the Ru(0001) metal surface. The peak at 2100 cm^{-1} was not observed after oxygen pre-exposure and subsequent CO adsorption at 100 K. The only peaks observed were at 2058 and 2042 cm^{-1}, attributed to the CO adsorbed on Rh and Ru metal, respectively. Interestingly, the 2058 cm^{-1} CO for the Ru-supported Rh was lower than that observed for the CeO_2-supported Rh (at 2075 cm^{-1}), suggesting that the adsorbed O and the CeO_2 together affected either the structure or the electronic response of the Rh islands or weakened the Rh–CO bonding.

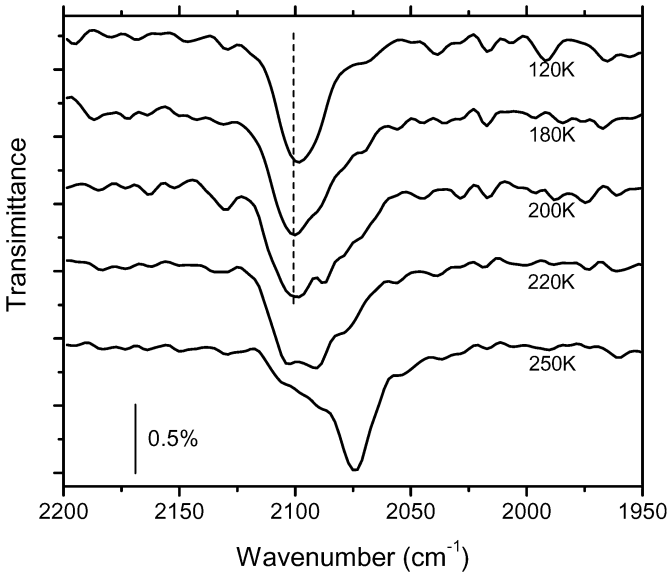

Fig. 4. IRAS spectra as a function of annealing temperature for CO adsorbed on O_2 pre-exposed Rh/CeO_2. Oxygen pre-exposure was 1.2 L and was performed at 300 K, before cooling to 110 K for the CO exposure. All spectra were measured at the temperature of 120 K after annealing at the indicated temperature for 30 s.

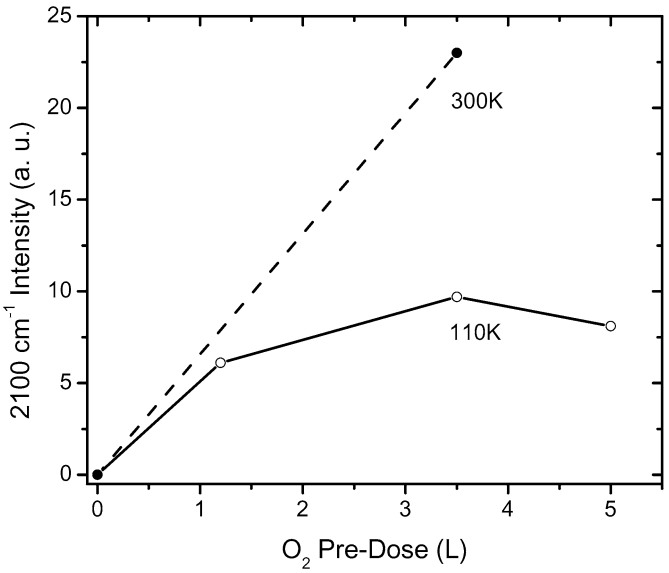

Fig. 5. Intensity of the 2100 cm^{-1} feature for CO adsorbed on Rh/CeO_2 and measured at 120 K as a function of O_2 pre-exposure at 110 K (open circles) or at 300 K (solid circles).

4. Discussion

The results indicate that two distinguishable states of CO occur on oxygen-pre-exposed Rh/CeO_2, these being *gem-*

Table 2
CO_2 desorption peak positions

Surface	Θ_{CO}[a]	Θ_O[a]	β_2 (K)	β_1 (K)	dT/dt (K/s)	References
Rh(111)			430	510	n/a	[9]
Rh(111)	0.22	0.17	n/a	450	5	[8]
Rh(111)	1.2[b]	2.1[b]	390	460	35	[2]
Rh(110)			430		n/a	[9]
Rh(100)	0.21	0.16	360	440	5	[8]
Poly Rh			280	410	48	[37]
Rh / CeO_2			290	360	3	Present results

[a] In Rh(111) monolayers.
[b] Exposure in Langmuirs.

dicarbonyl on dispersed Rh and linear CO on Rh island sites. Initially, the CeO_2(111) surface was covered with Rh islands that overlaid about half of the CeO_2 and are about two to three layers thick. On exposure of the Rh/CeO_2 surface to O_2, oxygen must interact with both Rh edge atoms around the periphery of the islands and with Rh "terrace" atoms on the top of islands. It is concluded that these two types of sites are responsible for the two different states of CO. When oxygen interacts with the edge of Rh islands, the edge atoms are dispersed into isolated Rh atoms that sense a stronger influence of the supporting CeO_2 than the large Rh islands. CO adsorption on these sites results in *gem*-dicarbonyl formation, as indicated by the 2100 cm^{-1} linear stretch frequency. As temperature increases in the range of 140–250 K, the isolated Rh aggregates into larger particles, and a portion of the CO from the dicarbonyl species desorbs from the surface. The remainder is converted to linear CO adsorption on Rh islands, giving rise to CO_2 formation at higher temperatures. For CO adsorbed on oxygen-covered Rh terraces, CO_2 formation is the dominant mechanism, similar to CO on an O_2-pre-exposed Rh single-crystal metal surface [2]. However, the CeO_2 also has an effect on these sites, causing a lowering of CO_2 formation temperature. CO ad-molecules immersed in O adsorption domains, give rise to β_2-CO_2 desorption. After a portion of the β_2-CO_2 desorbs, Rh sites become available for CO domains. The interaction of the CO at the edges of the O domains results in β_1-CO_2 formation/desorption.

It is reasonable to expect the edge Rh atoms to interact with oxygen in a different manner than the terrace Rh atoms because of the CeO_2 environment near the edge. Rh atoms in the edge are dispersed by oxygen to form small Rh particles with lower coordination. Many recent studies have shown that oxygen and CO can induce increased dispersion of metal particles supported on oxide surfaces [38–42]. The formation of isolated Rh atoms leads to formation of *gem*-dicarbonyl and a higher CO-stretching frequency. This picture is plausible because previous experiments conducted by Frank et al showed that smaller particles are correlated with formation of the *gem*-dicarbonyl [34]. The experimental results indicate that the CeO_2 support is needed for the formation of the *gem*-dicarbonyl. Exposure to oxygen at 300 K increases the dispersion of the edge sites compared with exposure at 110 K (Fig. 5).

For terrace sites, β_1 and β_2 CO_2 formation was observed at lower temperatures than typically reported for single-crystal metal surfaces. A summary of current and past results is given in Table 2. The table shows that the CO_2 formation temperatures observed in the present work are lower than those reported on single-crystal surfaces for comparable heating rates. But desorption temperatures for a polycrystalline surface and ceria-supported Rh particles are similar, both showing a β_2 peak below 300 K [37]. It is suggested that oxygen exposure of a Rh/CeO_2 surface induces a roughening in the Rh islands that facilitates the reaction between CO and O. Enhanced CO oxidation is possibly related to weakening of the bond between CO and Rh. Note that the observed shift of terrace CO-stretching frequency from 2066 to 2074 cm^{-1} requires both O-adsorption and CeO_2 support. Such a shift was not observed when the Rh islands were grown directly on Ru and then O_2 pre-exposed. This suggests that the CeO_2 support facilitates the oxygen-induced structural change in the Rh islands.

5. Conclusion

Oxygen exposure to CeO_2-supported Rh islands gives rise to two states of adsorbed CO, one leading to low temperature CO desorption and the other leading to CO_2 formation. The first state is characterized by desorption in the 140–250 K range and by a high stretching frequency of 2100 cm^{-1} observed in the same temperature range. This state is interpreted as dicarbonyl on small particles dispersed by the oxygen exposure on the supported Rh islands. The second state is characterized by CO_2 formation temperatures in the range of 290 K (β_2) to 360 K (β_1), and by a CO stretching frequency around 2074 cm^{-1}. This state is associated with adsorption at Rh terrace sites, which are modified slightly from those on low-index single-crystal Rh surfaces. Slightly lower CO_2 formation temperatures and a slightly higher CO stretching frequency are believed to be associated with a roughening in the Rh islands induced by the adsorbed oxygen and the CeO_2 support. For the range of Rh coverages studied, about 38–46% of the CO desorbs in the low-temperature state, while the remainder converts to CO_2.

Acknowledgments

This research was sponsored by the Division of Chemical Sciences, Geosciences, and Biosciences, Office of Basic Energy Sciences, US Department of Energy, under contract DE-AC05-00OR22725 with Oak Ridge National Laboratory, managed and operated by UT-Battelle, LLC. The authors acknowledge Jing Zhou for her assistance with the TPD equipment.

References

[1] M.J.P. Hopstaken, J.W. Niemantsverdriet, J. Chem. Phys. 115 (2001) 8209.
[2] T. Matsushima, T. Matsui, M. Hashimoto, J. Chem. Phys. 81 (1984) 5151.
[3] C.H.F. Peden, D.W. Goodman, D.S. Blair, P.J. Berlowitz, G.B. Fisher, S.H. Oh, J. Phys. Chem. 92 (1988) 1563.
[4] J. Yoshinobu, M. Kawai, J. Chem. Phys. 103 (1995) 3220.
[5] C.J. Zhang, P. Hu, J. Am. Chem. Soc. 122 (2000) 2134.
[6] S.B. Schwartz, L.D. Schmidt, G.B. Fisher, J. Phys. Chem. 90 (1986) 6194.
[7] B.A. Gurney, L.J. Richter, J.S. Villaruubia, W. Ho, J. Chem. Phys. 87 (1987) 6710.

[8] M.J.P. Hopstaken, J.W. Niemantsverdriet, J. Chem. Phys. 113 (2000) 5457.
[9] M. Bowker, Q. Guo, Y. Li, R.W. Joyner, Catal. Lett. 18 (1993) 119.
[10] A.J. Jaworowski, A. Beutler, F. Strislan, R. Nyholm, B. Setlik, D. Heskett, J.N. Andersen, Surf. Sci. 431 (1999) 33.
[11] A. Beutler, E. Lundgren, R. Nyholm, J.N. Andersen, B. Setlik, D. Heskett, Surf. Sci. 371 (1997) 381.
[12] A. Baraldi, S. Lizzit, D. Cocco, G. Comelli, G. Paolucci, R. Rosei, M. Kiskinova, Surf. Sci. 385 (1997) 376.
[13] L. Kohler, G. Kresse, M. Schmid, E. Lundgren, J. Gustafson, A. Mikkelsen, M. Borg, J. Yuhara, J.N. Andersen, M. Marsman, P. Varga, Phys. Rev. Lett. 93 (2004) 266103.
[14] L.-W.H. Leung, J.-W. He, D.W. Goodman, J. Chem. Phys. 93 (1990) 8328.
[15] L. Kohler, G. Kresse, Phys. Rev. B 70 (2004) 165405.
[16] L.H. Dubois, G.A. Somorjai, Surf. Sci. 91 (1980) 514.
[17] R. Linke, D. Curulla, M.J.P. Hopstaken, J.W. Niemantsverdriet, J. Chem. Phys. 115 (2001) 8209.
[18] D. Curulla, R. Linke, A. Clotet, J.M. Ricart, J.W. Niemantsverdreit, Chem. Phys. Lett. 354 (2002) 503.
[19] V. Fiorin, M.R.S. McCoustra, M.A. Chesters, J. Phys. Chem. B 107 (2003) 7058.
[20] A.L. Haller, D.C. Resasco, Adv. Catal. 36 (1989) 173.
[21] S.H. Overbury, D.R. Mullins, in: A. Trovarelli (Ed.), Catalysis by Ceria and Related Systems, vol. 2, Imperial College Press, 2001, p. 311.
[22] D.R. Mullins, S.H. Overbury, J. Catal. 188 (1999) 340.
[23] E.S. Putna, R.J. Gorte, J.M. Vohs, G.W. Graham, J. Catal. 178 (1998) 598.
[24] J. Stubenrauch, J.M. Vohs, J. Catal. 159 (1996) 50.
[25] R.M. Ferrizz, T. Egami, J.M. Vohs, Surf. Sci. 465 (2000) 127.
[26] S.H. Overbury, D.R. Mullins, L. Kundakovic, Surf. Sci. 470 (2001) 243.
[27] B. Jenewein, M. Fuchs, K. Hayek, Surf. Sci. 532 (2003) 364.
[28] B. Yoon, H. Hakkinen, U. Landman, A.S. Worz, J.-M. Antonietti, S. Abbet, K. Judai, U. Heiz, Science 307 (2005) 403.
[29] D.R. Mullins, S.H. Overbury, D.R. Huntley, Surf. Sci. 409 (1998) 307.
[30] J. Xu, S.H. Overbury, J. Catal. 222 (2004) 167.
[31] E.D. Williams, W.H. Weinberg, Surf. Sci. 82 (1979) 93.
[32] P.A. Thiel, E.D. Williams, J.T. Yates, W.H. Weinberg, Surf. Sci. 84 (1979) 54.
[33] P. Basu, D. Panayoyov, J.J.T. Yates, J. Am. Chem. Soc. 110 (1988) 2074.
[34] M. Frank, R. Kuhnemuth, M. Baumer, H.-J. Freund, Surf. Sci. 427–428 (1999) 288.
[35] S. Schwegmann, H. Over, V.D. Renzi, G. Ertl, Surf. Sci. 375 (1997) 91.
[36] G. Blyholder, J. Phys. Chem. 68 (1964) 2772.
[37] T. Matsushima, J. Catal. 83 (1983) 446.
[38] A. Berko, G. Menesi, F. Solymosi, J. Phys. Chem. 100 (1996) 17732.
[39] J. Evans, B. Hayden, F. Mosselmans, A. Murray, Surf. Sci. Lett. 279 (1992) L159.
[40] A. Kolmakov, D.W. Goodman, Catal. Lett. 70 (2000) 93.
[41] J. Zhou, Y.C. Kang, D.A. C. J. Phys. Chem. B 107 (2003) 6664.
[42] J. Zhou, Y.C. Kang, S. Ma, D.A. Chen, Surf. Sci. 562 (2004) 113.